Draft version July 7, 2020
Typeset using LaTeX **twocolumn** style in AASTeX63

Spin Dynamics in Hierarchical Black Hole Triples: Predicting Final Spin-Orbit Misalignment Angle From Initial Conditions

Yubo Su,[1] Dong Lai,[1] and Bin Liu

[1] *Cornell Center for Astrophysics and Planetary Science, Department of Astronomy, Cornell University, Ithaca, NY 14853, USA*

(Received XXXX; Revised XXXX; Accepted XXXX)

Submitted to ApJL

ABSTRACT

Abstract

Keywords: keywords

1. INTRODUCTION

This problem is important.

In Section 2, we set up the relevant equations of motion for the orbital and spin evolution of the three BHs, and we argue for the primary result of the paper, conservation of the angle θ_e. In Sections 3 and 4, we consider two scenarios under which conservation of θ_e can be violated. We discuss and conclude in Section 5.

2. ANALYTICAL SETUP

2.1. *Orbital Evolution*

We study Lidov-Kozai (LK) oscillations due to an external perturber to quadrupole order and include precession of pericenter and gravitational wave radiation due to general relativity. Consider an inner black hole (BH) binary with masses m_1 and m_2 having total mass m_{12} and reduced mass μ orbited by a third BH with mass m_3. Call a_3 the orbital semimajor axis of the third BH from the center of mass of the inner binary, and e_3 the eccentricity of its orbit, and define effective semimajor axis

$$\tilde{a}_3 \equiv a_3\sqrt{1-e_3^2}. \tag{1}$$

For simplicity, we adopt the test particle approximation such that the orbit of the third mass is fixed[1]. Call $\mathbf{L}_{\rm out} \equiv L_{\rm out}\hat{\mathbf{L}}_{\rm out}$ the fixed angular momentum of the outer BH relative to the center of mass of the inner BH binary, and call $\mathbf{L} \equiv L\hat{\mathbf{L}}$ the orbital angular momentum of the inner BH binary.

Corresponding author: Yubo Su
yubosu@astro.cornell.edu

[1] At quadrupole order, including the back-reaction terms is equivalent to considering LK oscillations of the inner binary about a fixed total angular momentum axis rather than $\mathbf{L}_{\rm out}$ (see e.g. Liu & Lai 2017, 2018).

We then consider the motion of the inner binary, described by orbital elements Keplerian orbital elements $(a, e, \Omega, I, \omega)$. The equations describing the motion of these orbital elements are (Peters 1964; Storch & Lai 2015; Liu & Lai 2018)

$$\frac{{\rm d}a}{{\rm d}t} = \left(\frac{{\rm d}a}{{\rm d}t}\right)_{\rm GW}, \tag{2}$$

$$\frac{{\rm d}e}{{\rm d}t} = \frac{15}{8t_{\rm LK}}e\sqrt{1-e^2}\sin 2\omega\sin^2 I + \left(\frac{{\rm d}e}{{\rm d}t}\right)_{\rm GW}, \tag{3}$$

$$\frac{{\rm d}\Omega}{{\rm d}t} = \frac{3}{4t_{\rm LK}}\frac{\cos I\left(5e^2\cos^2\omega - 4e^2 - 1\right)}{\sqrt{1-e^2}} + \Omega_{\rm GR}, \tag{4}$$

$$\frac{{\rm d}I}{{\rm d}t} = \frac{15}{16}\frac{e^2\sin 2\omega\sin 2I}{\sqrt{1-e^2}}, \tag{5}$$

$$\frac{{\rm d}\omega}{{\rm d}t} = \frac{3}{4t_{\rm LK}}\frac{2\left(1-e^2\right) + 5\sin^2\omega(e^2 - \sin^2 I)}{\sqrt{1-e^2}}, \tag{6}$$

where we define

$$t_{\rm LK}^{-1} = n\left(\frac{m_3}{m_{12}}\right)\left(\frac{a}{\tilde{a}_3}\right)^3, \tag{7}$$

$$\left(\frac{{\rm d}a}{{\rm d}t}\right)_{\rm GW} = -\frac{a}{t_{\rm GW}}, \tag{8}$$

$$= \frac{64}{5}\frac{G^3\mu m_{12}^2}{c^5a^3}\frac{1}{\left(1-e^2\right)^{7/2}}\left(1 + \frac{73}{24}e^2 + \frac{37}{96}e^4\right), \tag{9}$$

$$\left(\frac{{\rm d}e}{{\rm d}t}\right)_{\rm GW} = -\frac{304}{15}\frac{G^3\mu m_{12}^2}{c^5a^4}\frac{1}{\left(1-e^2\right)^{5/2}}\left(1 + \frac{121}{304}e^2\right), \tag{10}$$

$$\Omega_{\rm GR} = \frac{3Gnm_{12}}{c^2a\left(1-e^2\right)}, \tag{11}$$

and $n = \sqrt{Gm_{12}/a^3}$ is the mean motion of the inner binary. We will often refer to $e_{\rm min}$ and $e_{\rm max}$ the minimum/maximum

eccentricity in a single LK cycle, and we will sometimes notate $j = \sqrt{1-e^2}$ and $j_{\rm min} = \sqrt{1-e_{\rm max}^2}$.

Finally, for concreteness, we adopt fiducial parameters mirroring those from Liu & Lai (2018): the inner binary has $a = 100$ AU, $m_1 = 30M_\odot$, $m_2 = 20M_\odot$, and initial $e_0 = 0.001$ with varying I_0, while the tertiary companion has $\tilde{a}_3 = 4500$ AU, $m_3 = 30M_\odot$.

2.2. *Spin Dynamics: An Approximate Adiabatic Invariant*

We are ultimately interested in the spin orientations of the inner BHs at merger as a function of initial conditions. Since they evolve independently to leading post-Newtonian order, we focus on the dynamics of a single BH spin vector $\mathbf{S} = S\hat{\mathbf{S}}$. Neglecting spin-spin interactions, $\hat{\mathbf{S}}$ undergoes de Sitter precession about $\mathbf{L}$ as

$$\frac{{\rm d}\hat{\mathbf{S}}}{{\rm d}t} = \Omega_{\rm SL}\hat{\mathbf{L}}\times\hat{\mathbf{S}}, \tag{12}$$

$$\Omega_{\rm SL} = \frac{3Gn\,(m_2+\mu/3)}{2c^2a\left(1-e^2\right)}. \tag{13}$$

To analyze the dynamics of the spin vector, we go to co-rotating frame with $\hat{\mathbf{L}}$ about $\hat{\mathbf{L}}_{\rm out}$. Choose $\hat{\mathbf{L}}_{\rm out} = \hat{\mathbf{z}}$, and choose the $\hat{\mathbf{x}}$ axis such that $\hat{\mathbf{L}}$ lies in the x-z plane. In this coordinate system, Eq. (12) becomes

$$\left(\frac{{\rm d}\mathbf{S}}{{\rm d}t}\right)_{\rm rot} = \left(-\frac{{\rm d}\Omega}{{\rm d}t}\hat{\mathbf{z}} + \Omega_{\rm SL}\hat{\mathbf{L}}\right)\times\hat{\mathbf{S}}, \tag{14}$$

$$= \boldsymbol{\Omega}_{\rm e}\times\hat{\mathbf{S}}, \tag{15}$$

$$\boldsymbol{\Omega}_{\rm e} \equiv \Omega_{\rm L}\hat{\mathbf{z}} + \Omega_{\rm SL}\left(\cos I\hat{\mathbf{z}} + \sin I\hat{\mathbf{x}}\right), \tag{16}$$

$$\Omega_{\rm L} \equiv -\frac{{\rm d}\Omega}{{\rm d}t}. \tag{17}$$

In general, Eq. (15) is difficult to analyze, since $\Omega_{\rm L}$, $\Omega_{\rm SL}$ and I all vary significantly within each LK period, and we are interested in the final outcome after many LK periods. However, if we assume $t_{\rm GW} \gg t_{\rm LK}$, then the system can be treated as nearly periodic within each LK cycle. We can then rewrite Eq. (15) in Fourier components

$$\left(\frac{{\rm d}\hat{\mathbf{S}}}{{\rm d}t}\right)_{\rm rot} = \left[\overline{\boldsymbol{\Omega}}_{\rm e} + \sum_{N=1}^{\infty}\boldsymbol{\Omega}_{\rm eN}\cos\left(\frac{2\pi Nt}{P_{\rm LK}}\right)\right]\times\hat{\mathbf{S}}. \tag{18}$$

The bar denotes an average over an LK cycle. We adopt convention where $t = 0$ is the maximum eccentricity phase of the LK cycle.

We next assume that the $N \geq 1$ harmonics vanish exactly when the equation of motion is averaged over an LK cycle. This gives

$$\left(\frac{{\rm d}\hat{\bar{\mathbf{S}}}}{{\rm d}t}\right)_{\rm rot} = \overline{\boldsymbol{\Omega}}_{\rm e}\times\hat{\bar{\mathbf{S}}}. \tag{19}$$

Eq. (19) suggests that $\theta_{\rm e}$, given by

$$\cos\theta_{\rm e} \equiv \hat{\bar{\mathbf{S}}}\cdot\hat{\overline{\boldsymbol{\Omega}}}_{\rm e}, \tag{20}$$

is an adiabatic invariant. The adiabaticity condition requires the precession axis evolve slowly compared to the precession frequency at all times:

$$\left|\frac{{\rm d}\hat{\overline{\boldsymbol{\Omega}}}_{\rm e}}{{\rm d}t}\right| \ll \left|\overline{\boldsymbol{\Omega}}_{\rm e}\right|. \tag{21}$$

Since the orientation of $\overline{\boldsymbol{\Omega}}_{\rm e}$ changes on timescale $t_{\rm GW}$, we see that the adiabatic assumption is roughly equivalent to assuming each LK period can be Fourier decomposed [Eq. (18)].

To be more precise, we define the inclination angle $I_{\rm e}$ as the angle between $\overline{\boldsymbol{\Omega}}_{\rm e}$ and $\mathbf{L}_{\rm out}$ as shown in Fig. 2. Denoting also $\overline{\Omega}_{\rm e} \equiv \left|\overline{\boldsymbol{\Omega}}_{\rm e}\right|$, the adiabaticity condition can be expressed as

$$\frac{{\rm d}I_{\rm e}}{{\rm d}t} \ll \overline{\Omega}_{\rm e}. \tag{22}$$

Next, we express $I_{\rm e}$ in closed form. When the eccentricity is strongly oscillatory within each LK cycle (early in the evolution, see Fig. 1), we define averaged quantities

$$\overline{\Omega_{\rm SL}\sin I} \equiv \overline{\Omega}_{\rm SL}\sin\bar{I}, \tag{23}$$

$$\overline{\Omega_{\rm SL}\cos I} \equiv \overline{\Omega}_{\rm SL}\cos\bar{I}. \tag{24}$$

Then, using Eq.(16), we can see that

$$\tan I_{\rm e} = \frac{\bar{\mathcal{A}}\sin\bar{I}}{1+\bar{\mathcal{A}}\cos\bar{I}}, \tag{25}$$

where

$$\bar{\mathcal{A}} \equiv \frac{\overline{\Omega}_{\rm SL}}{\overline{\Omega}_{\rm L}}. \tag{26}$$

When eccentricity oscillations are suppressed at later times, we just have $\overline{\Omega}_{\rm SL} = \Omega_{\rm SL}$, $\overline{\Omega}_{\rm L} = \Omega_{\rm L}$, and $\bar{I} = I$.

3. ANALYSIS: DEVIATION FROM ADIABATICITY

In real systems, the particular extent to which $\theta_{\rm e}$ is conserved depends on how well Eq. (21) is satisfied. We will first present equations of motion for $\theta_{\rm e}$. We will then derive accurate estimates for important quantities in these equations of motion, and use these estimates to derive upper bounds on $\Delta\theta_{\rm e}$, the change in $\theta_{\rm e}$ over the entire inspiral. Taken together, this calculation estimates the deviation from adiabaticity as a function of initial conditions.

3.1. *Equation of Motion*

From the corotating frame [Eq. (19)], consider going to the reference frame where $\hat{\mathbf{z}}' = \hat{\overline{\boldsymbol{\Omega}}}_{\rm e}$ by rotation $-\dot{I}_{\rm e}\hat{\mathbf{y}}$. In this reference frame, the polar coordinate is just $\theta_{\rm e}$ as defined above in Eq. (20), and the equation of motion becomes

$$\left(\frac{{\rm d}\hat{\mathbf{S}}}{{\rm d}t}\right)' = \overline{\Omega}_{\rm e}\hat{\mathbf{z}}'\times\hat{\mathbf{S}}' - \dot{I}_{\rm e}\hat{\mathbf{y}}'\times\hat{\mathbf{S}}'. \tag{27}$$

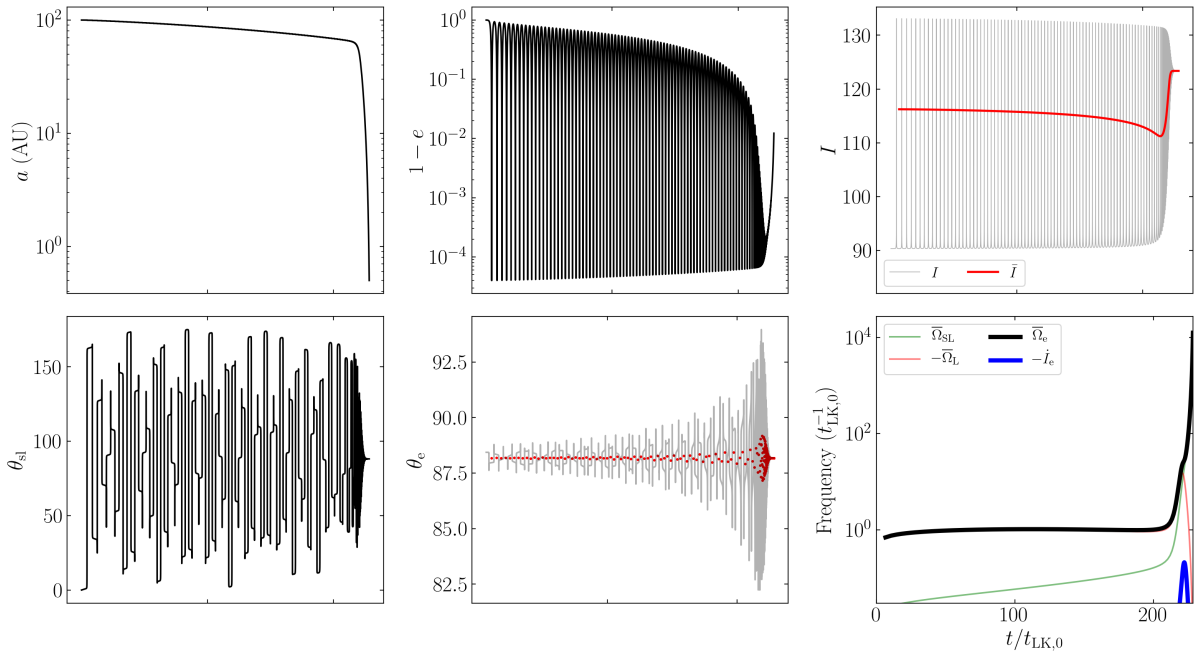

Figure 1. Orbital and spin evolution in a system for which the total change in the adiabatic invariant $\theta_{\rm e}$ is $\lesssim 0.01°$. The inner binary is taken to have $a = 100$ AU, $m_1 = 30M_\odot$, $m_2 = 20M_\odot$, $I_0 = 90.35°$, and $e_0 = 0.001$, while the tertiary companion has $\tilde{a}_3 = 4500$ AU, $m_3 = 30M_\odot$. The top three panels a; e; and the inclination of the inner binary, both instantaneous (I) and appropriately averaged following Eq. (24) ($\bar{I}$). The bottom three panels show the instantaneous spin-orbit misalignment angle $\theta_{\rm sl}$; the angle between $\overline{\mathbf{\Omega}}_{\rm e}$ [Eq. (16)] and both the instantaneous spin vector (light grey) and the LK-averaged spin vector [red dots, denoted $\theta_{\rm e}$, Eq. (20)]; and four characteristic frequencies of the system [Eqs. 16 and (17)]. The unit of time is the LK timescale [Eq. (7)] evaluated for the initial conditions $t_{\rm LK,0}$.

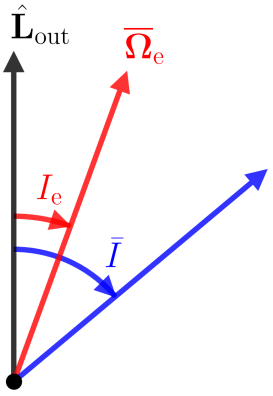

Figure 2. Definition of angles, shown in plane of the two angular momenta $\mathbf{L}_{\rm out}$ and $\mathbf{L}$, or the $\hat{\mathbf{x}}$–$\hat{\mathbf{z}}$ plane in the corotating frame. Note that for $I > 90°$, $I_{\rm e} < 0$.

If we break $\hat{\mathbf{S}}'$ into components $\hat{\mathbf{S}}' = S_x'\hat{\mathbf{x}}' + S_y'\hat{\mathbf{y}}' + \cos\theta_{\rm e}\hat{\mathbf{z}}'$ and define complex variable

$$S_\perp \equiv S_x' + iS_y', \tag{28}$$

we can rewrite Eq. 27 as

$$\frac{{\rm d}S_\perp}{{\rm d}t} = i\left(\overline{\Omega}_{\rm e}\right) S_\perp - \dot{I}_{\rm e}\cos\theta_{\rm e}. \tag{29}$$

This can be solved in closed form using an integrating factor. Defining

$$\Phi(t) \equiv \int^t \overline{\Omega}_{\rm e}\,{\rm d}t, \tag{30}$$

we obtain solution until final time $t_{\rm f}$

$$e^{-i\Phi}S_\perp\Big|_{-\infty}^{t_{\rm f}} = -\int_{-\infty}^{t_{\rm f}} e^{-i\Phi(\tau)}\dot{I}_{\rm e}\cos\theta\,{\rm d}\tau. \tag{31}$$

It can be seen that, in the adiabatic limit [Eq. (22)], $|S_\perp| = \sin\theta_{\rm e}$ is conserved over timescales $\gg 1/\overline{\Omega}_{\rm e}$, as the phase of the integrand in the right hand side varies much faster than the magnitude.

Recalling $|S_\perp| = \sin\theta_{\rm e}$ and analyzing Eq. (31), we see that $\sin\theta_{\rm e} \approx \theta_{\rm e}$ oscillates about its value at $t = -\infty$ with amplitude

$$|\Delta\theta_{\rm e}| \sim \frac{\dot{I}_{\rm e}}{\overline{\Omega}_{\rm e}}. \tag{32}$$

This is compared to the $\Delta\theta_{\rm e}$ from simulations in the bottom center panels of Figs. 3 and 4 as the green line. We see that in the latter simulation, the faster merger, the order of magnitude of $|\Delta\theta_{\rm e}|$ is somewhat well predicted, while in the slower merger a second contribution dominates $\Delta\theta_{\rm e}$ oscillations, discussed in Section 4.

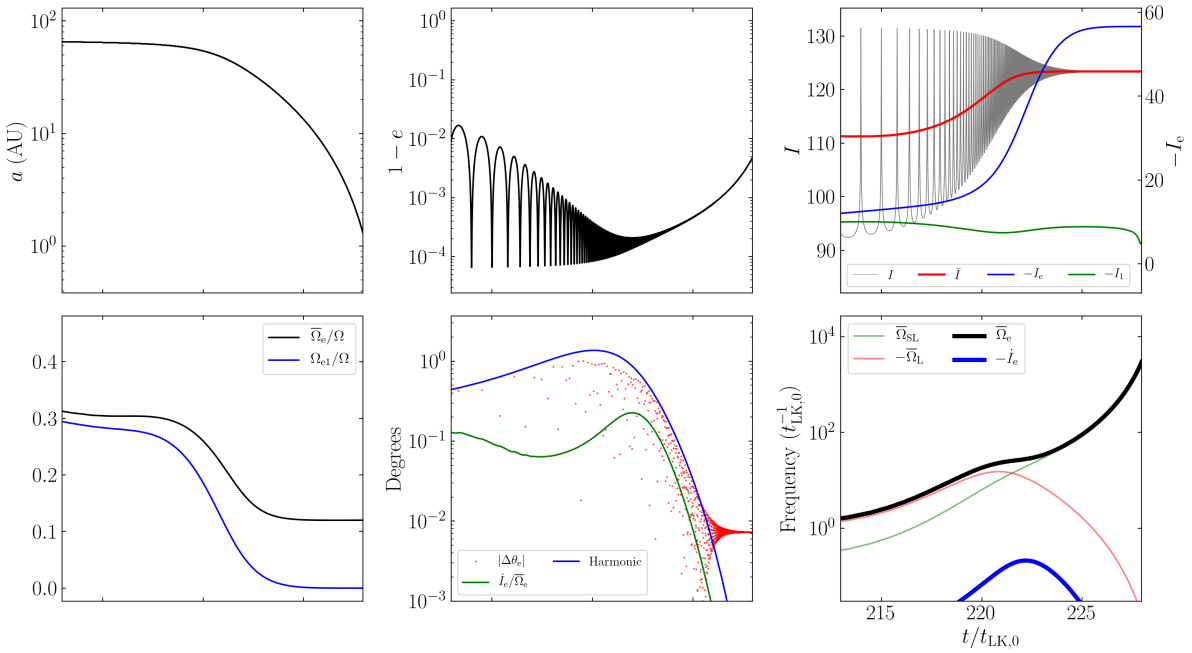

Figure 3. The same simulation as Fig. 1 but shown focusing on the region where $\bar{\mathcal{A}} \simeq 1$. The top three panels depict a, e, I and $\bar{I}$ as before, but in addition I_e [Eq. (25)] and I_1 [Eq. (47)] are shown in the third panel. The bottom three panels depict the frequency ratios between the zeroth and first Fourier components of $\mathbf{\Omega}_e$ to the LK frequency $\Omega = 2\pi/P_{LK}$; the magnitude of oscillation of θ_e away from its initial value (red dots) as well as amplitude estimates due to non-adiabatic effects [green, Eq. (32)] and due to resonances with harmonic terms [blue, Eq. (52)]; and the same characteristic frequencies as before. In the bottom middle panel, it is clear that oscillations in θ_e are dominantly driven by interactions with the $N = 1$ harmonic.

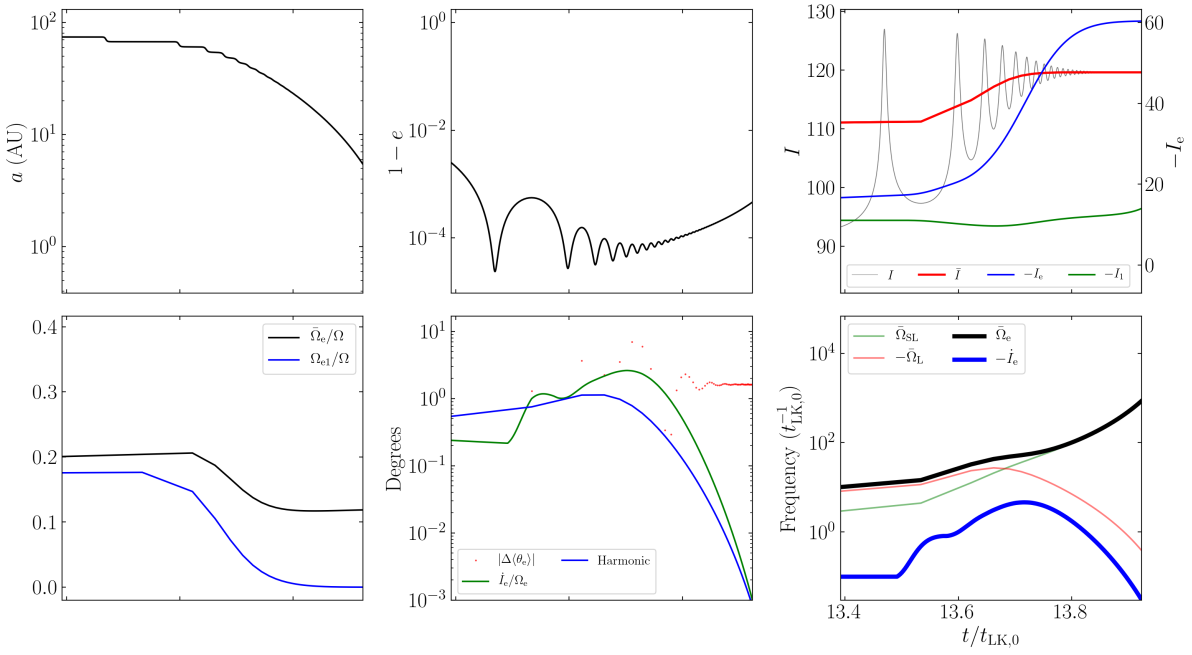

Figure 4. Same as Fig. 3 except for $I_0 = 90.2°$, corresponding to a faster merger and a total change in θ_e of $\approx 2°$. In the bottom middle panel, the nonadiabatic contribution is more significant and causes much poorer conservation of θ_e.

Furthermore, if we denote $\Delta\theta_{\rm e}^{(f)}$ to be the total change in $\theta_{\rm e}$ from $t=-\infty$ to merger, we can give loose bound[2]

$$\left|\Delta\theta_{\rm e}^{(f)}\right| \lesssim \left|\frac{\dot{I}_{\rm e}}{\overline{\Omega}_{\rm e}}\right|_{\rm max}. \tag{33}$$

In the following section, we show that this value can be calculated to good accuracy from initial conditions.

3.2. *Estimate of Deviation from Adiabaticity*

Towards estimating $\left[\dot{I}_{\rm e}/\overline{\Omega}_{\rm e}\right]_{\rm max}$, we first differentiate Eq. (25),

$$\dot{I}_{\rm e} = \left(\frac{\dot{\bar{\mathcal{A}}}}{\bar{\mathcal{A}}}\right)\frac{\bar{\mathcal{A}}\sin\bar{I}}{1+2\bar{\mathcal{A}}\cos\bar{I}+\bar{\mathcal{A}}^2}. \tag{34}$$

It also follows from Eq. (16) that

$$\overline{\Omega}_{\rm e} = \overline{\Omega}_{\rm L}\left(1+2\bar{\mathcal{A}}\cos\bar{I}+\overline{\mathcal{A}}^2\right)^{1/2}, \tag{35}$$

from which we obtain

$$\left|\frac{\dot{\bar{I}}_{\rm e}}{\overline{\Omega}_{\rm e}}\right| = \left|\frac{\dot{\bar{\mathcal{A}}}}{\bar{\mathcal{A}}}\right|\frac{1}{\left|\overline{\Omega}_{\rm L}\right|}\frac{\bar{\mathcal{A}}\sin\bar{I}}{\left(1+2\bar{\mathcal{A}}\cos\bar{I}+\bar{\mathcal{A}}\right)^{3/2}}. \tag{36}$$

This is maximized when $\bar{\mathcal{A}}\simeq 1$, and so we obtain that the maximum deviation should be bounded by

$$\left|\frac{\dot{I}_{\rm e}}{\overline{\Omega}_{\rm e}}\right|_{\rm max} \simeq \left|\frac{\dot{\bar{\mathcal{A}}}}{\bar{\mathcal{A}}}\right|\frac{1}{\left|\overline{\Omega}_{\rm L}\right|}\frac{\sin\bar{I}}{\left(2+2\cos\bar{I}\right)^{3/2}}. \tag{37}$$

To evaluate this, we make two assumptions: (i) $\bar{I}$ is approximately constant, and (ii) $j_{\rm min}=\sqrt{1-e_{\rm max}^2}$ evaluated at $\bar{\mathcal{A}}\simeq 1$ is some constant multiple of the initial $j_{\rm min}$, so that

$$j_\star \equiv (j)_{\bar{\mathcal{A}}\simeq 1} = f\sqrt{\frac{5}{3}\cos^2 I_0}, \tag{38}$$

for some unknown factor $f>1$; we use star subscripts to denote evaluation at $\bar{\mathcal{A}}\simeq 1$. f turns out to be relatively insensitive to I_0. This can be as systems with lower $e_{\rm max}$ values take more cycles to attain $\bar{\mathcal{A}}\simeq 1$ and thus experience a similar amount of decay due to GW radiation.

For simplicity, let's first assume $\bar{\mathcal{A}}\simeq 1$ is satisfied when the LK oscillations are mostly suppressed, and $e_\star\approx 1$ throughout the LK cycle (we will later see that the scalings are the same in the LK-oscillating regime). Then we can write

$$\bar{\mathcal{A}} \simeq \frac{3Gn\,(m_2+\mu/3)}{2c^2 a j^2}\left[\frac{3\cos\bar{I}}{4t_{\rm LK}}\frac{1+3e^2/2}{j}\right]^{-1}, \tag{39}$$

$$\simeq \frac{G(m_2+\mu/3)m_{12}\tilde{a}_3^3}{c^2 m_3 a^4 j\cos\bar{I}}, \tag{40}$$

$$\propto \frac{1}{a^4 j}, \tag{41}$$

$$\frac{\dot{\bar{\mathcal{A}}}}{\bar{\mathcal{A}}} = -4\left(\frac{\dot{a}}{a}\right)_{\rm GW} + \frac{e}{j^2}\left(\frac{{\rm d}e}{{\rm d}t}\right)_{\rm GW}. \tag{42}$$

Approximating $e_\star\approx 1$ in Eqs. (9) and (10) gives

$$\left[\frac{\dot{\bar{\mathcal{A}}}}{\bar{\mathcal{A}}}\right]_{\bar{\mathcal{A}}=1} \simeq \frac{64G^3\mu m_{12}^2}{5c^5 a_\star^4 j_\star^7}\times 15, \tag{43}$$

$$\overline{\Omega}_{{\rm L},\star} \approx \frac{3\cos\bar{I}}{2t_{\rm LK} j_\star}, \tag{44}$$

$$\left|\frac{\dot{\bar{I}}_{\rm e}}{\overline{\Omega}_{\rm e}}\right|_{\rm max} \approx \frac{128G^3\mu m_{12}^2}{c^5 a_\star^4 j_\star^6}\frac{t_{\rm LK}}{\cos\bar{I}}\frac{\sin\bar{I}}{\left(2+2\cos\bar{I}\right)^{3/2}}. \tag{45}$$

With the ansatz for $j_\star$ given by Eq. (38) and requiring Eq. (40) equal 1 for a given $j_\star$ and $a_\star$ gives us the final expression

$$\left|\frac{\dot{\bar{I}}_{\rm e}}{\overline{\Omega}_{\rm e}}\right|_{\rm max} \approx \frac{128G^3\mu m_{12}^3\tilde{a}_3^3}{c^5\sqrt{Gm_{12}}m_3}\left(\frac{c^2 m_3\cos\bar{I}}{G(m_2+\mu/3)m_{12}\tilde{a}_3^3}\right)^{11/8} \times (j_\star)^{-37/8}\frac{\tan\bar{I}}{\left(2+2\cos\bar{I}\right)^{3/2}}. \tag{46}$$

The agreement of Eq. (46) with numerical simulation is remarkable, as shown in Fig. 5.

Above, we assumed that $\bar{\mathcal{A}}\simeq 1$ is satisfied when the eccentricity is mostly constant (see Fig. 1 for an indication of how accurate this is for the parameter space explored in Fig. 5). It is also possible that $\bar{\mathcal{A}}\simeq 1$ occurs when the eccentricity is still undergoing substantial oscillations. In fact, Eq. (46) is still accurate in this regime when replacing e with $e_{\rm max}$, due to the following analysis. When $e_{\rm min}\ll e_{\rm max}$, the binary spends a fraction $\sim j_{\rm min}$ of the LK cycle near $e\simeq e_{\rm max}$ (Anderson et al. 2016). This fraction of the LK cycle dominates both GW dissipation and $\overline{\Omega}_{\rm L}$ precession. Thus, both $\dot{\bar{\mathcal{A}}}$ and $\overline{\Omega}_{\rm L}$ in Eq. (37) are evaluated at $e\approx e_{\rm max}$ and are suppressed by a factor of $j_{\rm min}$. However, $\dot{\bar{\mathcal{A}}}$ and $\overline{\Omega}_{\rm L}$ appear in the numerator and denominator of Eq. (46) respectively, and so the $j_{\rm min}$ factors cancel. In conclusion, when the eccentricity is still substantially oscillating, Eq. (46) remains accurate when e is replaced with $e_{\rm max}$.

The accuracy of Eq. (46) in bounding the total change in $\Delta\theta_{\rm e}^{(f)}$ over inspiral is shown in Fig. 6. Note that conservation of $\theta_{\rm e}$ is generally much better than Eq. (46) predicts; cancellation of phases in Eq. (31) is generally more efficient than Eq. (46) assumes.

[2] Given the complicated evolution of $\overline{\Omega}_{\rm e}$ and $\dot{I}_{\rm e}$, it is difficult to give a more exact bound on the deviation from adiabaticity. In practice, deviations $\lesssim 1^\circ$ are observationally indistinguishable, so the exact scaling in this regime is negligible.

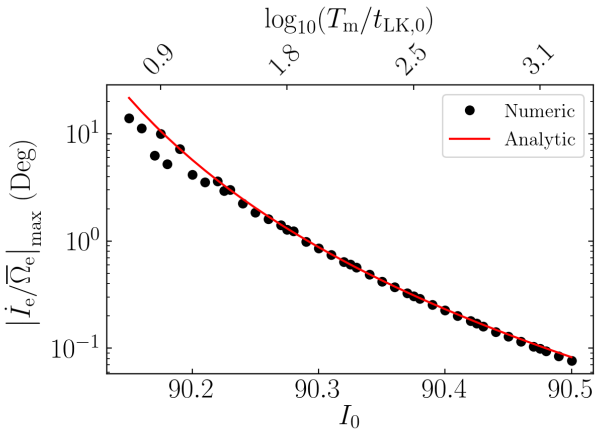

Figure 5. Comparison of $\left|\dot{\vec{I}}_e/\overline{\Omega}_e\right|_{max}$ extracted from simulations and using Eq. (46), where we take $f = 2.6$ in Eq. (38). The merger time P_m is shown along the top axis of the plot in units of the characteristic LK timescale at the start of inspiral $t_{LK,0}$; the LK period is initially of order a few $t_{LK,0}$. The agreement is remarkable for mergers that are more adiabatic (towards the right).

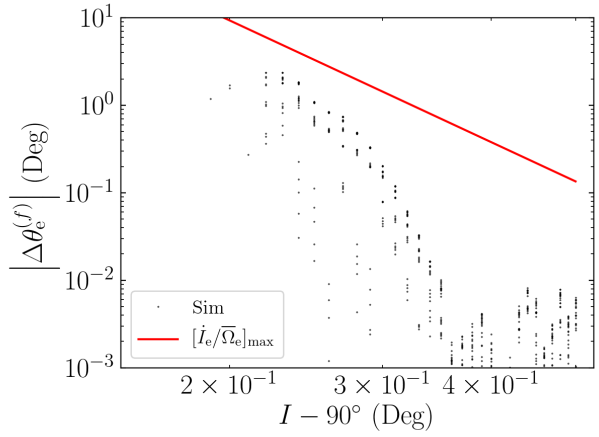

Figure 6. Change in θ_e over inspiral as a function of initial inclination I_0. Plotted for comparison is the bound $\left|\Delta\theta_e^{(f)}\right| \lesssim \left|\dot{I}_e/\overline{\Omega}_e\right|_{max}$, given by Eq. (46). It is clear that the given bound is not tight but provides an upper bound for non-conservation of θ_e due to nonadiabatic effects. The leftmost portion of this plot is less reliable as the quasi-periodic assumption within each LK cycle breaks down as GW dissipation within each LK cycle is substantial.

4. ANALYSIS: RESONANCES AND BREAKDOWN OF θ_E CONSERVATION

In the previous section, we assumed the $N \geq 1$ Fourier harmonics in Eq. (18) are negligible when averaging over an LK period. However, this assumption breaks down near resonances. For simplicity, we ignore the effects of GW dissipation in this section and assume the system is exactly periodic. For each $\mathbf{\Omega}_{eN}$ Fourier harmonic [defined in Eq. (18)], denote its magnitude Ω_{eN} and its inclination angle relative to $\mathbf{L}_{out}$ as I_N, using the same convention as Fig. 2. We then rewrite Eq. (18) in component form in the reference frame where $\hat{\mathbf{z}}' \propto \overline{\mathbf{\Omega}}_e$:

$$\left(\frac{d\hat{\mathbf{S}}}{dt}\right)' = \overline{\Omega}_e \hat{\mathbf{z}}' \times \hat{\mathbf{S}}' + \left[\sum_{N=1}^{\infty} \Omega_{eN} \cos(N\Omega t)\left(\cos(\Delta I_N)\hat{\mathbf{z}}' + \sin(\Delta I_N)\hat{\mathbf{x}}'\right)\right] \times \hat{\mathbf{S}}'. \tag{47}$$

Here, $\Delta I_N \equiv I_e - I_N$ and $\Omega = 2\pi/P_{LK}$ is the LK angular frequency. Following a similar procedure to Section 3.1, we obtain an equation analogous to Eq. (31):

$$\frac{dS_\perp}{dt} = i\left(\overline{\Omega}_e + \Omega_{eN}\cos(\Delta I_N)\cos N\Omega t\right) S_\perp - i\cos\theta \sin(\Delta I_N)\,\Omega_{eN}\cos N\Omega t. \tag{48}$$

In this equation, there are potentially resonances when $\overline{\Omega}_e = N\Omega$. Since, $\overline{\Omega}_e \lesssim \Omega$ for most regions of parameter space (see Fig. 7), we restrict our analysis to resonances with the $N = 1$ component. The two possible resonant behaviors are a parametric resonance [modulation of the oscillation frequency in Eq. (48)] and resonant forcing by the second term. Parametric resonances are typically very narrow and are therefore hard to excite as the system's frequencies change under GW dissipation. As such, we consider only the effect of the second term in Eq. (48).

Restricting our attention to $N = 1$ and neglecting the parametric term, the equation of motion reduces to

$$\frac{dS_\perp}{dt} \approx i\overline{\Omega}_e S_\perp - i\cos\theta_e \sin(\Delta I_N)\,\Omega_{eN}\cos(N\Omega t). \tag{49}$$

We can approximate $\cos(N\Omega t) \approx e^{iN\Omega t}/2$, as the $e^{-iN\Omega t}$ component is far from resonance. Then we can write down solution

$$\Phi(t) = \int^t \overline{\Omega}_e\, d\tau, \tag{50}$$

$$e^{-i\Phi} S_\perp\Big|_{-\infty}^{\infty} = -\int_{-\infty}^{\infty} \frac{i\sin(\Delta I_1)\,\Omega_{e1}}{2} e^{-i\Phi(\tau)+i\Omega\tau}\cos\theta_e\, d\tau. \tag{51}$$

Thus, similarly to Section 3.1, $|\Delta\theta_e|$ can be bound by

$$|\Delta\theta_e| \sim \frac{1}{2}\frac{\sin(\Delta I_1)\,\Omega_{e1}}{\Omega - \overline{\Omega}_e}. \tag{52}$$

This is shown as the blue line in the bottom center panels of Fig. 3 and 4. We see that the amplitude of oscillations in θ_e

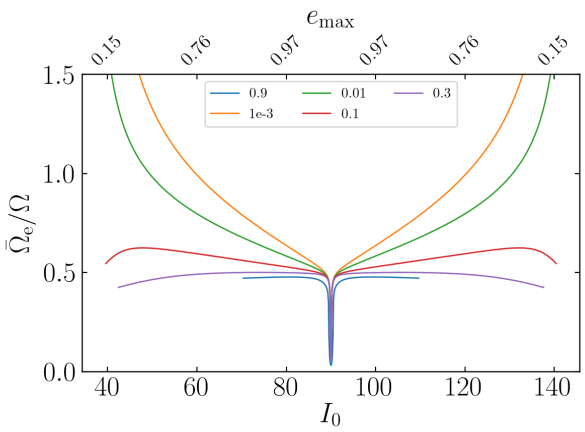

Figure 7. For the fiducial set of parameters, $\overline{\Omega}_e/\Omega$ as a function of I_0 (corresponding to $e_{\max}$ labeled on top axis) for varying values of $e_{\min}$. Both smaller $e_{\min}$ and $e_{\max}$ values more easily satisfy the resonant condition $\overline{\Omega}_e/\Omega \approx 1$. Data are only shown when $e_{\min} < e_{\max}$.

are well described by Eq. (52), particularly in the former case (where the non-adiabatic contribution is weaker).

Again analogously to Section 3.1, we obtain loose bound for total nonconservation of θ_e

$$\left|\Delta\theta_e^{(f)}\right| \lesssim \left[\frac{\sin(\Delta I_1)\,\Omega_{e1}}{\Omega - \overline{\Omega}_e}\right]_{\max}. \tag{53}$$

While Eq. (52) depends on the properties of the $N = 1$ Fourier component, the condition for substantial θ_e nonconservation can be understood in terms of physical quantities:

- $\sin(\Delta I_1)$ is small unless $\bar{\mathcal{A}} \simeq 1$. Otherwise, $\mathbf{\Omega}_e$ does not nutate appreciably within an LK cycle, and all the $\mathbf{\Omega}_{eN}$ are aligned with $\overline{\mathbf{\Omega}}_e$, implying all the $\Delta I_N \approx 0$.
- Smaller values of both $e_{\min}$ and $e_{\max}$ increase $\overline{\Omega}_e/\Omega$, as shown in Fig. 7, strengthening the interaction with the $N = 1$ resonance.

LK-driven coalescence causes $\bar{\mathcal{A}}$ to increase on a similar timescale to that of $e_{\min}$ increase (see Fig. 1). As such, we conclude that the effect of harmonic terms generally only affects θ_e conservation when $\bar{\mathcal{A}} \approx 1$ initially.

5. CONCLUSION AND DISCUSSION

Relation between θ_e and $\theta_{sl}^{(f)}$, as a function of I.

The "chaotic" behavior in Paper I is because it satisfies the heuristic provided at the end of the harmonics section well.

Interestingly, harmonic terms begin to dominate $\Delta\theta_e$ at quite small inclinations $I_0 \lesssim 90.35°$, but the non-adiabatic contribution to nonconservation obviously dominates out to $I_0 \approx 90.4°$.

REFERENCES

Anderson, K. R., Storch, N. I., & Lai, D. 2016, Monthly Notices of the Royal Astronomical Society, 456, 3671

Liu, B., & Lai, D. 2017, The Astrophysical Journal Letters, 846, L11

—. 2018, The Astrophysical Journal, 863, 68

Peters, P. C. 1964, Physical Review, 136, B1224

Storch, N. I., & Lai, D. 2015, Monthly Notices of the Royal Astronomical Society, 448, 1821